

# Self-Doped Mixed Ionic-Electronic Conductors to Tune the Threshold Voltage and the Mode of Operation in Organic Electrochemical Transistors

Julian Hungenberg, Adrian Hochgesang, Florian Meichsner, and Mukundan Thelakkat\*

Organic mixed ionic-electronic conductors with tunable doping, low threshold voltages, and air stability are crucial for bioelectronic applications. A homopolymer based on an alkoxy thiophene monomer and its copolymer with a thiophene carrying ethylene glycol side chains are synthesized and converted to self-doped conjugated polyelectrolytes, P3HOTS-TMA<sup>+</sup>, and P3HOTS-TMA<sup>+</sup>-co-P3MEEET. The self-doping occurs during the conversion to polyelectrolytes. Both polyelectrolytes show high electrical conductivity without any external dopants. UV-Vis-NIR spectroscopy and spectroelectrochemistry confirm excellent air stability of the doped state. In an organic electrochemical transistor (OECT), the P3HOTS-TMA<sup>+</sup> operates in depletion mode, while P3HOTS-TMA<sup>+</sup>-co-P3MEEET exhibits accumulation mode of operation with low threshold voltage, both showing fast response times. On the other hand, the non-doped homopolymer, P3MEEET, shows a high negative threshold voltage in accumulation mode. Thus, copolymerization with the self-dopable monomer changes the mode of operation as well as the threshold voltage substantially. Ultraviolet photoelectron spectroscopy reveals a considerable reduction of the hole injection barrier for the self-doped system P3HOTS-TMA<sup>+</sup>. Mott-Schottky analysis shows reduction in charge carrier concentration in the copolymer compared to the homopolymer. Thus, the copolymerization strategy with a self-dopable monomer is an efficient tool for tuning the degree of doping leading to low threshold voltage in OECTs.

conductors (OMIECs) have emerged as highly suitable active materials in organic electrochemical transistors (OECTs).<sup>[1,2]</sup> OECTs are electronic devices whose key feature comprises the conversion of low input electric current via low gate voltage applied through an electrolyte into high current amplifications between the source and drain electrodes. Such transistors operate at low voltage (<1 V), often in aqueous electrolytes, which is why they have been widely used especially in bioelectronics as sensors,<sup>[3]</sup> or in bioelectronic circuits<sup>[4,5]</sup> of neuromorphic devices like artificial synapses and neurons.<sup>[6–8]</sup> OECTs can either work in accumulation mode (using pristine OMIECs) or depletion mode (using heavily doped OMIECs).<sup>[9,10]</sup> For p-type OMIECs working in accumulation mode, the transistor is initially in the OFF state, but it is switched ON when a negative gate voltage is applied. When there is an additional applied voltage between the source and the drain electrode, the source-drain current,  $I_D$  of the OECT can be measured in accumulation mode. With p-type material working in depletion mode, the operation is vice versa. The OECT is initially ON

## 1. Introduction


Due to their ability to interact with ions in aqueous media as well as their semiconducting nature, organic mixed ionic-electronic

and is turned OFF when a positive gate voltage is applied. Therefore, the depletion mode shows disadvantages such as high power consumption, and consequently, its applicability for biosensing applications or in inverter circuits is disfavored.<sup>[11–13]</sup>

Although it operates in depletion mode, the commercially available poly(3,4-ethylenedioxythiophene) polystyrene sulfonate (PEDOT:PSS) is still the state-of-the-art material for OECTs. It consists of the conjugated polymer PEDOT in its doped state (PEDOT<sup>+</sup>), surrounded and stabilized by insulating PSS<sup>-</sup> counterions. Due to its heavily doped nature, OECTs using PEDOT:PSS as channel material have high power consumption in the equilibrium state. On the other hand, for any system, a high threshold voltage ( $V_T$ ) above 0.5 V in an aqueous medium can cause device instability during operation due to possible parasitic side-reaction with water and oxygen. For bioelectronics, a low  $V_T$  for OECT is of particular interest since it reduces power consumption, minimizes the voltage stress of living biological cells upon application, and suppresses such side reactions.<sup>[14,15]</sup>

J. Hungenberg, A. Hochgesang, F. Meichsner  
Applied Functional Polymers University of Bayreuth  
Universitätsstr. 30, 95447 Bayreuth, Germany

M. Thelakkat  
Applied Functional Polymers and Bavarian Polymer Institute  
University of Bayreuth  
Universitätsstr. 30, 95447 Bayreuth, Germany  
E-mail: [mukundan.thelakkat@uni-bayreuth.de](mailto:mukundan.thelakkat@uni-bayreuth.de)

 The ORCID identification number(s) for the author(s) of this article can be found under <https://doi.org/10.1002/adfm.202407067>

© 2024 The Author(s). Advanced Functional Materials published by Wiley-VCH GmbH. This is an open access article under the terms of the [Creative Commons Attribution-NonCommercial](https://creativecommons.org/licenses/by-nc/4.0/) License, which permits use, distribution and reproduction in any medium, provided the original work is properly cited and is not used for commercial purposes.

DOI: 10.1002/adfm.202407067

Consequently, innovative OMIECs are urgently needed to provide low- $V_T$  OECT devices working ideally in accumulation mode. In general, many OMIECs in accumulation mode work under high threshold voltages above 0.4 V in OECTs.<sup>[5,16,17]</sup> To address this issue, Keene et al. demonstrate that by using aliphatic amines as reducing agents for PEDOT:PSS, OECTs having low  $V_T$  in accumulation mode can be realized.<sup>[18]</sup> Doris et al. used different redox couples to control the electrochemical potential at the gate electrode, thereby causing a direct shift of  $V_T$ .<sup>[19]</sup> Recently, Tseng and coworkers have tuned the threshold voltage  $V_T$  in PEDOT:PSS devices by using a dual gate approach to apply in complementary inverters.<sup>[20]</sup> In another study, Tan et al. reported a reasonable shift in  $V_T$  of accumulation mode devices with polythiophene with ethylene glycol side chains p(g3T2) as active material, employing chemically doped OMIEC gate electrodes.<sup>[21]</sup> Besides these approaches, it is essential to mention that  $V_T$  is primarily governed by the semiconductor and its doping levels, more precisely by its electronic properties such as the ionization potential (IP) and the Fermi level ( $E_F$ ). Therefore, chemical modification of semiconductor polymer structures, their side chains, and the degree of doping are potential tools to tailor these parameters.<sup>[22–24]</sup> Furthermore, for applications in aqueous medium, these OMIECs have to be not only air-stable in the pristine (undoped) form, but also in the doped state.

However, only a few examples of doped OMIEC systems other than PEDOT:PSS have been reported. Examples are based on self-doped conjugated polyelectrolytes (CPEs) on which charges of the doped conjugated backbone are self-compensated by the polymer side chains bearing ionic groups so that external ions such as the insulating PSS<sup>-</sup> can be avoided.<sup>[25]</sup> These CPEs include self-doped PEDOT derivatives and alkoxy-substituted polythiophene derivatives, which are synthesized by oxidative polymerization or electro-polymerization and they are water-soluble. In contrast to these self-doped systems, PEDOT:PSS is a blend of two polymers, which form a stabilized dispersion in aqueous or polar solvents. They also have high electrical conductivities from 0.5–3000 S cm<sup>-1</sup>.<sup>[26–32]</sup> Beaumont et al. demonstrate the synthesis of a series of self-doped polythiophene homo- and copolymers by direct heteroarylation polymerization (DHAP) as an alternative to the less controlled oxidative synthesis methods.<sup>[33]</sup> Besides polythiophenes, a self-doped donor-acceptor copolymer polyelectrolyte based on benzothiadiazole has also been reported for OECTs.<sup>[34–36]</sup>

In this work, we present a new route to self-doped (and self-compensated) polythiophenes by well-controlled polymerization technique Kumada catalyst transfer polymerization followed by polymer analogous conversion to polyelectrolytes carrying sulfonate salts in the side chains. During the conversion into polyelectrolytes, the system is in situ doped and the charges on the backbone are self-compensated by counter ions on the side chain. This self-doped CPE homopolymer (P3HOTS<sup>-</sup>TMA<sup>+</sup>) features an alkoxy-linked side chain on thiophene to reduce its ionization potential, resulting in a high electrical conductivity with air-stability. It also operates in depletion mode when applied in a p-type OECT. We show that the degree of doping can be precisely tuned by copolymerization with a not self-dopable comonomer (2,5-dibromo-3-(2-(2-methoxyethoxy)ethoxy)ethyl)thiophene, (3MEEET), which changes the OECT operation from depletion to accumulation

mode. On the other hand, if both the accumulation mode materials, the self-doped copolymer and the undoped P3MEEET are compared with each other, the threshold voltage could be considerably reduced in the copolymer. Thus, the presented strategy is versatile and highly flexible to tune the fundamental characteristics of OECTs.

## 2. Results and Discussion

The new alkoxy-substituted monomer 2,5-dibromo-3-((6-bromohexyl)oxy)thiophene, (3HOTBr) **3** was synthesized by a transesterification reaction starting from 3-methoxythiophene **1** followed by dibromination of the resulting thiophene derivative **2** (Figure 1a). All the experimental details and analytical data, such as the <sup>1</sup>H NMR spectra of the monomers (Figures S1 and S2, Supporting Information), can be found in the Supporting Information. We synthesized the second monomer, an ethylene glycol substituted thiophene, namely 2,5-dibromo-3-(2-(2-(2-methoxyethoxy)ethoxy)ethyl)thiophene, (3MEEET) **4**, according to a formerly published protocol.<sup>[37]</sup> Via Kumada catalyst-transfer polymerization (KCTP) the precursor homopolymer poly(3-(6-(bromohexyl)oxy)thiophene-2,5-diyl) (P3HOTBr) and the copolymer, poly[(3-(6-(bromohexyl)oxy)thiophene-2,5-diyl)-co-(3-(2-(2-(2-methoxyethoxy)ethoxy)ethyl)thiophene-2,5-diyl)] (P3HOTBr-co-P3MEEET) were synthesized (Figure 1c). KCTP is a well-known method for polymerizing 2,5-dibrominated alkyl thiophenes but is also suitable for alkoxy-substituted thiophenes resulting in low dispersity and very high regioregularity.<sup>[38–41]</sup> The KCTP procedure was adapted from a published protocol.<sup>[37,42]</sup> In preliminary experiments with THF as the solvent, the precipitation of P3HOTBr at low conversion was observed, presumably due to its poor solubility in THF. Therefore, to increase the solubility of the emerging precursor homopolymer and thus prevent precipitation during polymerization, we used a mixture of THF and 1,2-dichlorobenzene as solvent at relatively low monomer concentrations (0.05 M). The number average molecular weight is determined to be 7.5 kg mol<sup>-1</sup> with a dispersity  $\bar{D} = 1.3$  for the homopolymer P3HOTBr and 6.5 kg mol<sup>-1</sup> (and  $\bar{D} = 2.0$ ) for the copolymer P3HOTBr-co-P3MEEET as measured by gel permeation chromatography (GPC) using THF containing 0.25 wt.% tetrabutylammonium bromide as eluent and PS calibration (Figure 1b). Even though the salted eluent reduces aggregation and interaction of these special polymers with the stationary phase, the PS calibration can give only rough estimates for these thiophene-based polymers.<sup>[42]</sup>

In addition, the copolymer P3HOTBr-co-P3MEEET was synthesized via KCTP in a one-pot reaction with a monomer feed-in ratio 50:50 (mol%) of the monomers **3** and **4**, resulting in a built-in ratio of 60:40 mol% (3HOTBr:3MEEET) as obtained from <sup>1</sup>H-NMR analysis (Figure S3, Supporting Information). This higher incorporation of 3HOTBr compared to 3MEEET is probably due to a slightly higher reactivity of the alkoxy-substituted monomer **3** compared to **4**. The relative reactivities of monomers **3** and **4** and kinetics for the build-up of monomers in copolymerization are analyzed using <sup>1</sup>H-NMR analysis at different time intervals, as shown in Figure S4 (Supporting Information). This is supported by the gas chromatography analysis for different conversions, which shows the difference in the decrease of both monomer concentrations in the reaction

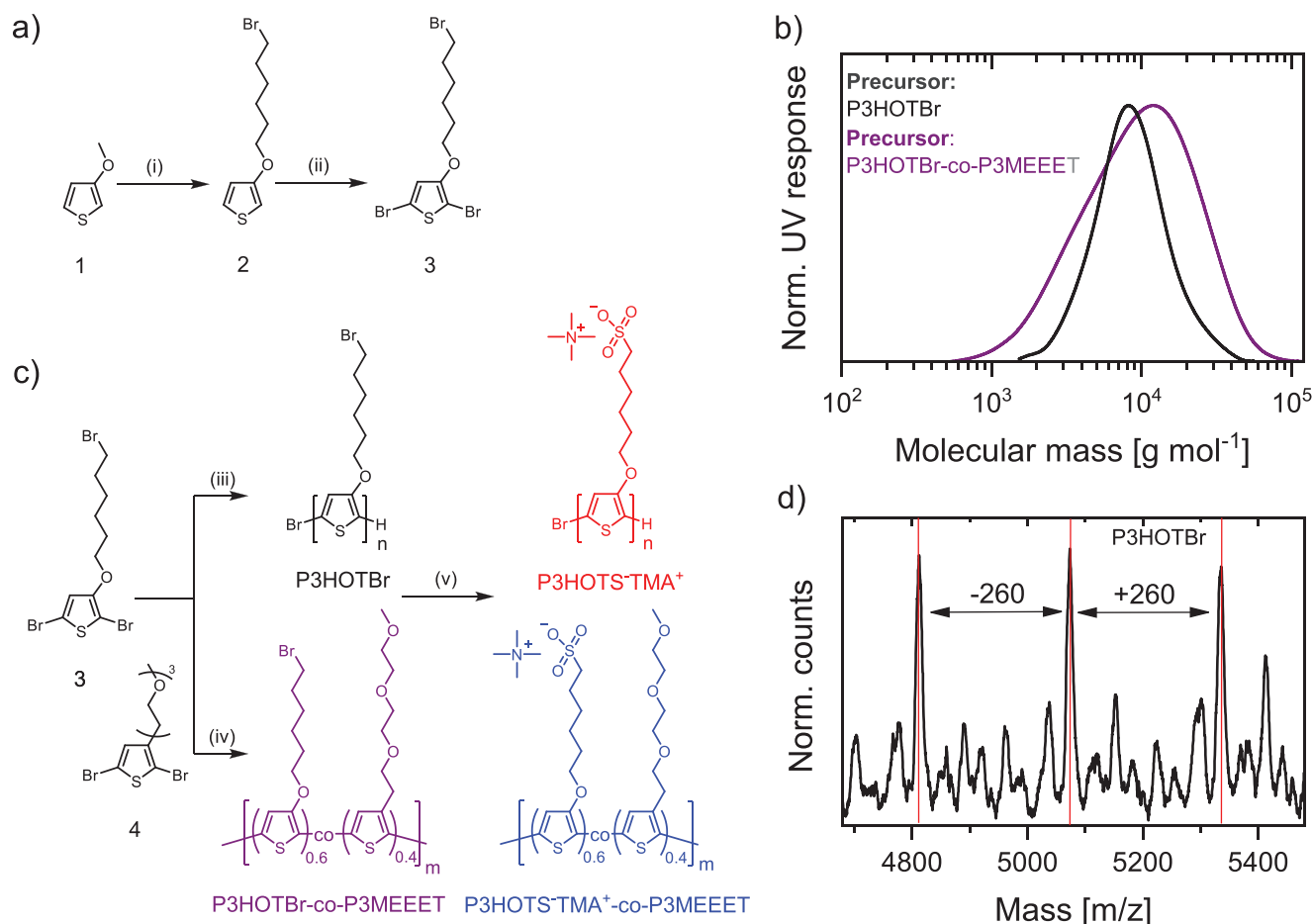


**Figure 1.** a) Synthetic route for the new dibrominated alkoxy-substituted monomer **3**: (i) 6-bromo-hexane-1-ol, *p*-TsOH, toluene, 90 °C; (ii) *N*-bromosuccinimide, THF/acidic acid; b) molecular weight distribution and dispersity of the precursor polymers via gel permeation chromatography in THF containing 0.25 wt.% tetrabutylammonium bromide and PS calibration; c) reaction scheme of the polymerization via Kumada catalyst transfer polymerization and the polymer analogous substitution: (iii) and (iv) *t*-BuMgCl, Ni(dppp)Cl<sub>2</sub>, THF/1,2-DCB, RT, (v) tetramethylammonium sulfite, 1,2-DCB/DMSO, RT; d) MALDI-ToF MS spectra for the precursor polymer P3HOTBr showing the exact mass for the repeating units of 3HOTBr in the main peak series of the detected polymer.

mixture over time (Figure S5, Supporting Information). Thus, the copolymerization yielded rather a random copolymer with some gradient characteristics since monomer **3** is consumed only slightly faster than monomer **4**. Matrix Assisted Laser Desorption Ionization-Time of Flight (MALDI-ToF) experiments provide further evidence for the successful formation of both precursor polymers (Figure 1d; Figure S6, Supporting Information). The final CPEs were obtained by polymer analogous substitution of the terminal bromine group with freshly prepared bis(tetramethylammonium) sulfite in a mixture of 1,2-DCB and DMSO (4:1 v/v). We used <sup>1</sup>H-NMR to provide proof for the complete conversion (Figure S7, Supporting Information). We allocate the singlet at 3.14 ppm to the methyl groups of the TMA<sup>+</sup> counterions. Besides this signal, no polymer-related signals are observed. We attribute this to the high degree of doping of the CPEs (forming radical salts) already after the polymer analogous conversion to polyelectrolytes and purification via dialysis and the resulting paramagnetism, which prevents the acquisition of <sup>1</sup>H-NMR of the backbone. In contrast to the precursor polymers, the resulting CPEs are fully soluble in water and methanol

(>10 mg mL<sup>-1</sup>), which is a further indication of a conversion from the terminal bromine to sulfonate having tetramethyl ammonium (TMA<sup>+</sup>) counterions (Figure S8, Supporting Information). Additionally, the homopolymer P3MEEET, a polythiophene with oligo ethylene glycol side chains (Figure S9, Supporting Information), was synthesized from monomer **4** as published to be used as a non-doped reference material.<sup>[37]</sup> Both CPEs show no thermal transition features in DSC experiments, which would indicate crystallization of the polymer chains (Figure S10, Supporting Information).

The UV-Vis-NIR absorbance spectra of thin films of P3HOTS<sup>-</sup>TMA<sup>+</sup>, as well as P3HOTS<sup>-</sup>TMA<sup>+</sup>-co-P3MEEET and their respective precursor polymers, P3HOTBr and P3HOTBr-co-P3MEEET, are shown in Figure 2a. Both the precursor polymers show only the  $\pi$ - $\pi^*$  absorption bands in the range of 620–640 nm, without any indication of polaron absorption in the longer wavelength region. However, both the homopolymer polyelectrolyte P3HOTS<sup>-</sup>TMA<sup>+</sup> as well as the copolymer polyelectrolyte P3HOTS<sup>-</sup>TMA<sup>+</sup>-co-P3MEEET show considerably bleached  $\pi$ - $\pi^*$  absorption, and simultaneously, two additional

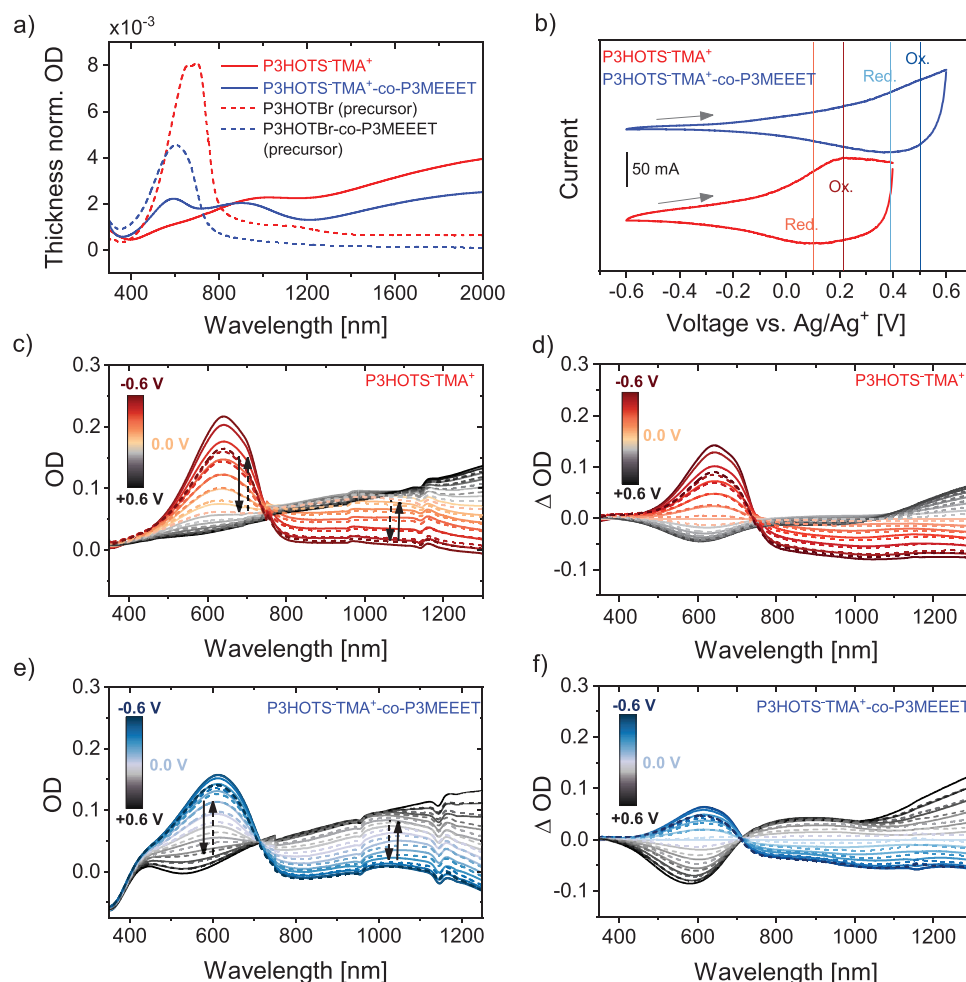


**Figure 2.** a) Optical density (OD) of UV–Vis–NIR spectra of both CPEs compared to their precursors in thin films on glass (normalized to the film thickness); b) cyclic voltammograms of undoped P3HOTS-TMA<sup>+</sup>, and P3HOTS-TMA<sup>+</sup>-co-P3MEEET as thin films on Pt sputtered ITO, at a scan rate of 50 mV s<sup>-1</sup> in acetonitrile containing 0.1 M TBAPF<sub>6</sub>; c,e) SEC spectra from -0.6 to +0.6 V (oxidation, solid lines) and +0.6 to -0.6 V (reduction, dashed lines); d,f) delta absorbance SEC spectra, for which the measured curve for an applied voltage of 0.0 V is subtracted from each curve. SEC curves were recorded on thin films on ITO in 0.1 M NaCl<sub>aq</sub> using a three-electrode setup with Ag/AgCl reference and Pt-counter electrode. The arrows denote the direction of alterations in the spectrum for the forward scan (solid arrows) and the backward scan (dashed arrows).

and broad absorption bands at higher wavelengths above 720 nm. The first broad band arising between  $\lambda = 720$  and 1220 nm can be assigned to polaronic features (doped state), as suggested for doped conjugated polymers.<sup>[43]</sup> Similarly, the second absorption band, observed between  $\lambda = 1220$  and 2000 nm might originate from the formation of bipolarons.<sup>[44]</sup> Similar observations were reported for other self-doped polythiophene derivatives by Beaumont et al.<sup>[33]</sup> For P3HOTS-TMA<sup>+</sup>, both the low energy feature absorptions are significantly more pronounced than for P3HOTS-TMA<sup>+</sup>-co-P3MEEET, which indicates a higher degree of p-doping in the former. This is understandable since the copolymer has only 60 mol% of the dopable monomer. The pronounced polaronic absorption in CPEs is accompanied by a concomitant bleaching of the  $\pi$ - $\pi^*$  absorption ( $\lambda = 370$ –720 nm). This is further shown in the comparison of the absorption spectra of the precursor polymers and those of the CPEs (Figure 2a). For comparison, the UV–Vis–NIR spectra of the homopolymer P3MEEET and PEDOT:PSS are also given in Figure S11a

(Supporting Information). The homopolymer P3MEEET shows an absorption band with vibronic features between  $\lambda = 400$  and 690 nm. Two distinct red-shifted vibronic transition peaks (0-0 and 0-1) are observed, indicating aggregation and excitonic coupling as reported for other polythiophenes.<sup>[42,45–48]</sup> Interestingly, the  $\pi$ - $\pi^*$  absorption of the copolymer P3HOTBr-co-P3MEEET does not show prominent aggregation features of the P3MEEET segment indicating the random sequence of the copolymer. Moreover, the UV–Vis–NIR absorption spectrum of P3HOTS-TMA<sup>+</sup> is very similar to that of PEDOT:PSS, which is also in a heavily doped state. The main difference in the doping of P3HOTS-TMA<sup>+</sup> and PEDOT:PSS is the lack of any external dopants in the former. Additionally, the comparison of the absorption of the respective precursor polymers with those of the CPEs clearly shows that the doping occurs during the introduction of the sulfonate group in the side chain via reaction with bis(tetramethylammonium) sulfite. During dialysis, any excess TMA<sup>+</sup> cation are removed to guarantee charge neutrality of



the self-doped system. We therefore conclude that the self-doped state of the CPEs is self-compensated by the negatively charged sulfonate groups in the side chain.<sup>[49]</sup> Furthermore, we stored these self-doped CPE films for two weeks in ambient conditions to investigate their aging stability (Figure S11b, Supporting Information). Interestingly, the absorbance between  $\lambda = 720$  and 1220 nm and  $\lambda = 1220$  and 2000 nm almost does not decrease, indicating a high stability of the self-compensated doped state in air.

We measured cyclic voltammograms (CV) of polymer thin films on Pt sputtered Indium Tin Oxide (ITO)<sub>8</sub> substrate in acetonitrile (Figure 2b; Figures S12 and S13, Supporting Information). All the samples were subjected to a reduction potential of  $-0.6$  V before measuring the oxidation potentials to de-dope them and make sure that the measured values correspond to pristine (undoped) polymers. P3HOTS·TMA<sup>+</sup> shows a redox couple with a halfway oxidation potential of 0.16 V versus Ag/AgNO<sub>3</sub>. For P3HOTS·TMA<sup>+</sup>-co-P3MEEET only a weak inflection point at  $\approx 0.45$  V and no clear oxidation peak was observed in CV measurements. Therefore, differential pulse voltammetry (DPV) measurements were carried out for both undoped polymers and oxidation peak potentials of 0.30 and 0.50 V versus Fc/Fc<sup>+</sup> were obtained (see Figure S14, Supporting Information). It is obvious both from CV and DPV measurements that the oxidation of the copolymer is shifted to higher voltages by  $\approx 0.2$ – $0.3$  V versus Fc/Fc<sup>+</sup>, which indicates a significantly easier oxidizability of the pristine homopolymer. We estimated the ionization potential (IP) values for the undoped samples based on the CV data by calibrating with the reference couple Fc/Fc<sup>+</sup> and using solvent corrections as reported elsewhere.<sup>[50]</sup> This results in IP =  $-4.87$  and  $-5.16$  eV for the undoped homopolymer and the copolymer, respectively. The reference homopolymer P3MEEET exhibits an IP =  $-5.27$  eV. Details are given in the Supporting Information (Figures S14 and S15 and Table S1, Supporting Information). The IP values estimated from CV must be considered as approximate values suitable only for a comparison. It is also observed that in DPV measurements, the peak onsets for P3HOTS·TMA<sup>+</sup> and P3HOTS·TMA<sup>+</sup>-co-P3MEEET are almost identical, with  $-0.31$  and  $-0.32$  V versus Fc/Fc<sup>+</sup>, respectively, indicating that the self-dopable moiety starts oxidizing at the same potential in both cases. However, for the P3MEEET homopolymer, the onset is shifted to a higher value of  $-0.09$  V versus Fc/Fc<sup>+</sup>, indicating the impact of the self-dopable moiety in the copolymer (Figures S14 and S15, Supporting Information).

To probe the changes in absorption of the polymers as a function of applied bias (electrochemical doping) in an aqueous electrolyte (0.1 M NaCl solution), we performed spectroelectrochemistry (SEC) experiments using a three-electrode setup. Figure 2c,e shows the UV–Vis–NIR absorbance spectra of P3HOTS·TMA<sup>+</sup> and P3HOTS·TMA<sup>+</sup>-co-P3MEEET for each applied potential, respectively. Figure 2d,f depicts the delta absorbance plots, in which the data for  $V = 0.0$  V versus Ag/AgCl is subtracted from each measured curve. We first applied a negative bias of  $V = -0.6$  V versus Ag/AgCl to reduce the self-doped polymer films fully. The corresponding spectra show a pronounced  $\pi$ – $\pi^*$  absorption band at  $\lambda = 640$  nm (for P3HOTS·TMA<sup>+</sup>) and  $\lambda = 620$  nm (for P3HOTS·TMA<sup>+</sup>-co-P3MEEET) with only negligible polaron absorption, indicating the polymers to be in the reduced state (compare Figure 2a). Upon the application of

oxidative biases in 100 mV steps, the  $\pi$ – $\pi^*$  absorption band bleaches completely at  $V = +0.6$  V with a concomitant increase of absorption bands at a higher wavelength (polaron formation) above an isosbestic point ( $\lambda_{\text{isosbestic, P3HOTS·TMA}^+} \approx 750$  nm and  $\lambda_{\text{isosbestic, P3HOTS·TMA}^+ \text{-co-P3MEEET}} \approx 715$  nm). The reversibility of the doping/de-doping process is shown by a backward scan from the fully doped state at  $V = +0.6$  V to the reduced state at  $V = -0.6$  V, depicted by the dashed lines. Thereby, the maximum  $\pi$ – $\pi^*$  absorption intensity regains 80% for P3HOTS·TMA<sup>+</sup> and 90% for P3HOTS·TMA<sup>+</sup>-co-P3MEEET. There is no onset for the electrochemical oxidation in SEC for both self-doped systems as the films are already in a partially self-doped state at  $V = 0$  V versus Ag/AgCl. This is also observed for the as-cast films, for which the UV–Vis–NIR spectra recorded at the beginning without applying a bias, indicates the high stability of the doped state even in the aqueous electrolyte (Figure S16, Supporting Information). Additionally, this is in accordance with the UV–Vis–NIR measurements, which clearly indicate the polaron peaks of the doped state.

Since films of both self-doped CPEs exist in partially doped/oxidized states without applying a potential in the dry state as well as in an aqueous electrolyte, we studied the self-doping behavior of an electrochemically reduced film in the presence of aqueous electrolyte in an SEC setup itself. For this, a reductive potential of  $V = -0.6$  V was applied to the films on ITO, and a UV–vis spectrum was recorded in the pristine state. Then, the bias was removed, and further spectra were recorded at different time intervals at zero bias for 120 min (Figure 3a,b). This study indicates that the de-doped state is not stable and the self-doped state is regained very fast within minutes. The homopolymer and the copolymer return to the original equilibrium self-doped states within 15 and 8 min respectively and no further self-doping/oxidation occurs. This is displayed in the plot of absorption intensity of the  $\pi$ – $\pi^*$  transition against time (Figure 3c). The data points were fitted using an exponential decay function (Equations S2 and S3, Supporting Information). Within the first 15 min, the  $\pi$ – $\pi^*$  absorption of the pristine forms decreases by 85% for P3HOTS·TMA<sup>+</sup> and by 30% for P3HOTS·TMA<sup>+</sup>-co-P3MEEET and corresponding polaronic features arise simultaneously. These observations indicate the high stability of these self-doped, self-compensated systems, which reverse back to their doped state under ambient conditions, even if they are forcefully reduced using applied bias. The self-compensation of the charges on the backbone is facilitated via the anionic side chains.

For a conjugated polymer in aqueous medium, there are different oxidants such as dissolved oxygen and H<sub>3</sub>O<sup>+</sup>, which can oxidize the de-doped state back to self-doped, self-compensated state. To understand if H<sup>+</sup> ions (possibly available in any aqueous electrolyte) dopes the reduced form, we studied the impact of the H<sup>+</sup> by collecting UV–vis–NIR spectra of these CPEs in buffer solutions from pH 2 to pH 10, and indeed, both polymers show a higher degree of doping with a decrease in pH toward highly acidic conditions (Figures S17a and S18, Supporting Information). Moreover, the degree of further doping in a highly acidic state is less pronounced for the homopolymer than for the copolymer. Besides protons, dissolved oxygen in the electrolyte could also act as the initial dopant.<sup>[41–53]</sup> It is conceivable that both effects occur here. The homopolymer with a higher number of self-dopable repeating units

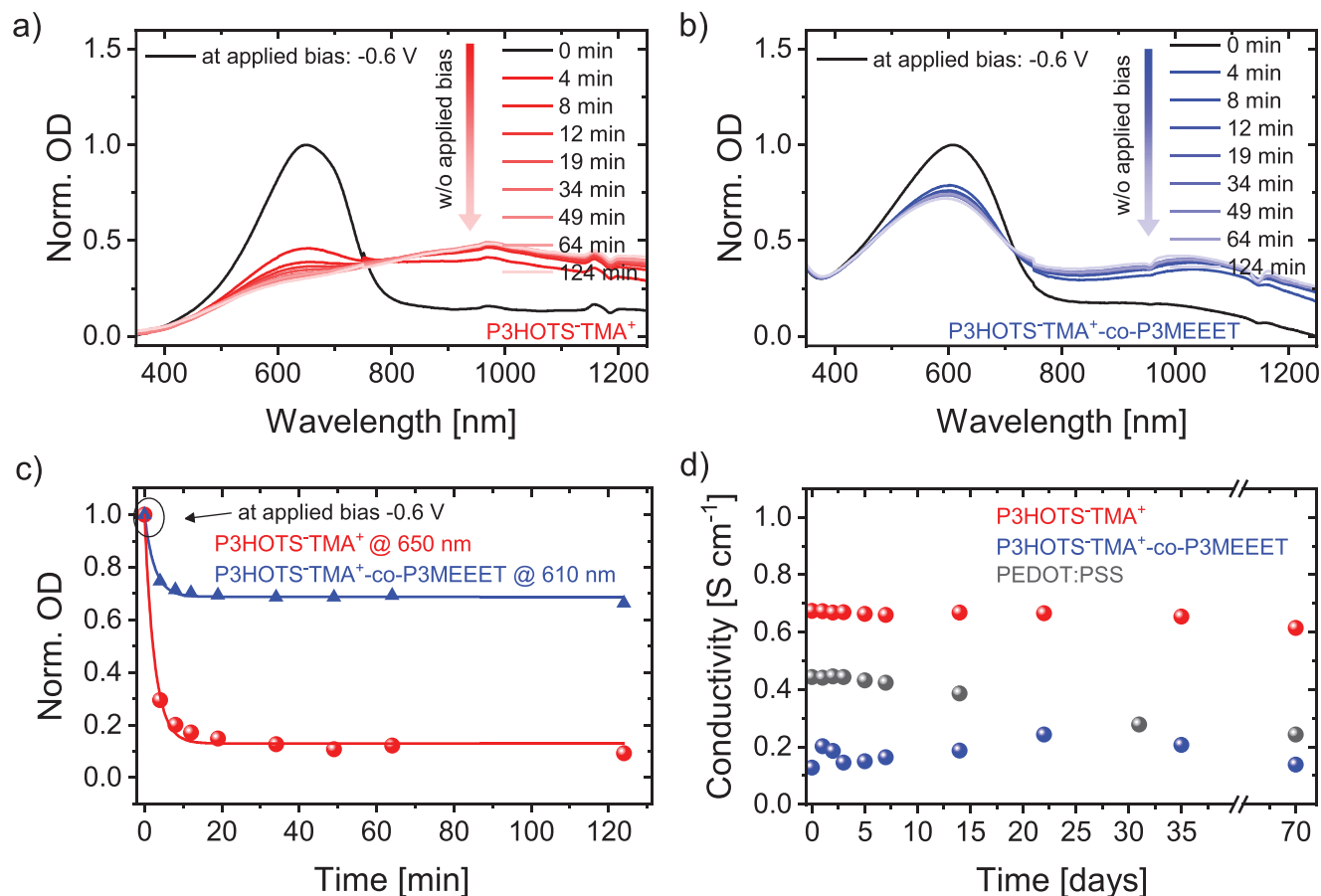


**Figure 3.** Optical density (OD) values for UV–vis–NIR spectral changes up to 124 min in thin films on ITO in 0.1 M NaCl<sub>aq</sub>. of a) P3HOTS-TMA<sup>+</sup> and b) P3HOTS-TMA<sup>+</sup>-co-P3MEEET after pre-reduction to pristine states in an electrochemical cell with a potential of −0.6 V versus Ag/AgCl; c) normalized optical density values showing the decrease of the  $\pi$ - $\pi^*$  absorption maxima at 650 and 610 nm for P3HOTS-TMA<sup>+</sup> and P3HOTS-TMA<sup>+</sup>-co-P3MEEET respectively (solid line represents the fit of the exponential decay function); d) Temporal changes in electrical conductivity of thin films of P3HOTS-TMA<sup>+</sup> and P3HOTS-TMA<sup>+</sup>-co-P3MEEET upon storage under atmospheric conditions.

(100 mol%) compared to the copolymer (60 mol%) can stabilize this self-doped states more effectively, which results in a higher polaron absorption intensity seen in the UV–vis–NIR spectra.

Measurements of the electrical conductivity (Figure 3d) by collecting  $I$ - $V$  curves of thin films on interdigitated gold electrodes revealed conductivities of  $\sigma = 0.67 \text{ S cm}^{-1}$  for a freshly cast film of the homopolymer P3HOTS-TMA<sup>+</sup> and  $\sigma = 0.13 \text{ S cm}^{-1}$  for the copolymer P3HOTS-TMA<sup>+</sup>-co-P3MEEET which is about seven orders of magnitude higher than for conventional undoped polythiophenes such as P3HT reported with  $\sigma_{\text{P3HT}} = 2 \times 10^{-8} \text{ S cm}^{-1}$ .<sup>[54]</sup> For a comparison the group of Bazan and Nguyen have reported a self-doped donor-acceptor benzothiadiazole cyclopentadithiophene CPE exhibiting electrical conductivity in the range of 0.0015 to 0.03 S cm<sup>-1</sup> in its as prepared state without using any oxidizing agents.<sup>[34–36]</sup>

Of course, higher conductivity values for CPEs are obtained by using additional oxidizing agents. Beaumont et al reported self-compensated CPEs based on PEDOT and alkoxy polythiophenes obtained by an additional oxidative step using cationic ion-exchange resin Dowex 50WX8 50–100 (H) exhibiting conductivity values in the range of 0.5–50 S cm<sup>-1</sup>.<sup>[33]</sup> Whereas,

self-compensated PEDOT polyelectrolytes obtained by Yano et al via an oxidative polymerization using strong external oxidizing agents such as (NH<sub>4</sub>)<sub>2</sub>S<sub>2</sub>O<sub>8</sub> (very similar to PEDOT:PSS) exhibit an electrical conductivity value of 1000 S cm<sup>-1</sup>.<sup>[29]</sup> On the other hand, the electrical conductivity of externally doped and stabilized systems such as PEDOT:PSS heavily depend on the degree of external doping, ratio of PEDOT:PSS, and the nature of stabilizing agent. It varies over a very broad range from 10<sup>-4</sup>–10<sup>3</sup> S cm<sup>-1</sup>.<sup>[55]</sup>

The high conductivity values obtained in our systems (without any added external oxidants) presumably originate from the high degree of self-doping, as shown above in the UV–Vis–NIR and SEC measurements. We assume that the higher conductivity of P3HOTS-TMA<sup>+</sup> is directly related to the higher degree of self-doping compared to P3HOTS-TMA<sup>+</sup>-co-P3MEEET. Further, the doped states are extremely stable under ambient conditions as shown by measuring the temporal electrical conductivity up to 70 days, whereby the films were stored in ambient atmospheric conditions in a closed vessel in the lab (Figure 3d). The change in conductivity as a function of time is given in the normalized conductivity plot in Figure S11b, Supporting Information). Remarkably, 91% of the initial conductivity of the freshly

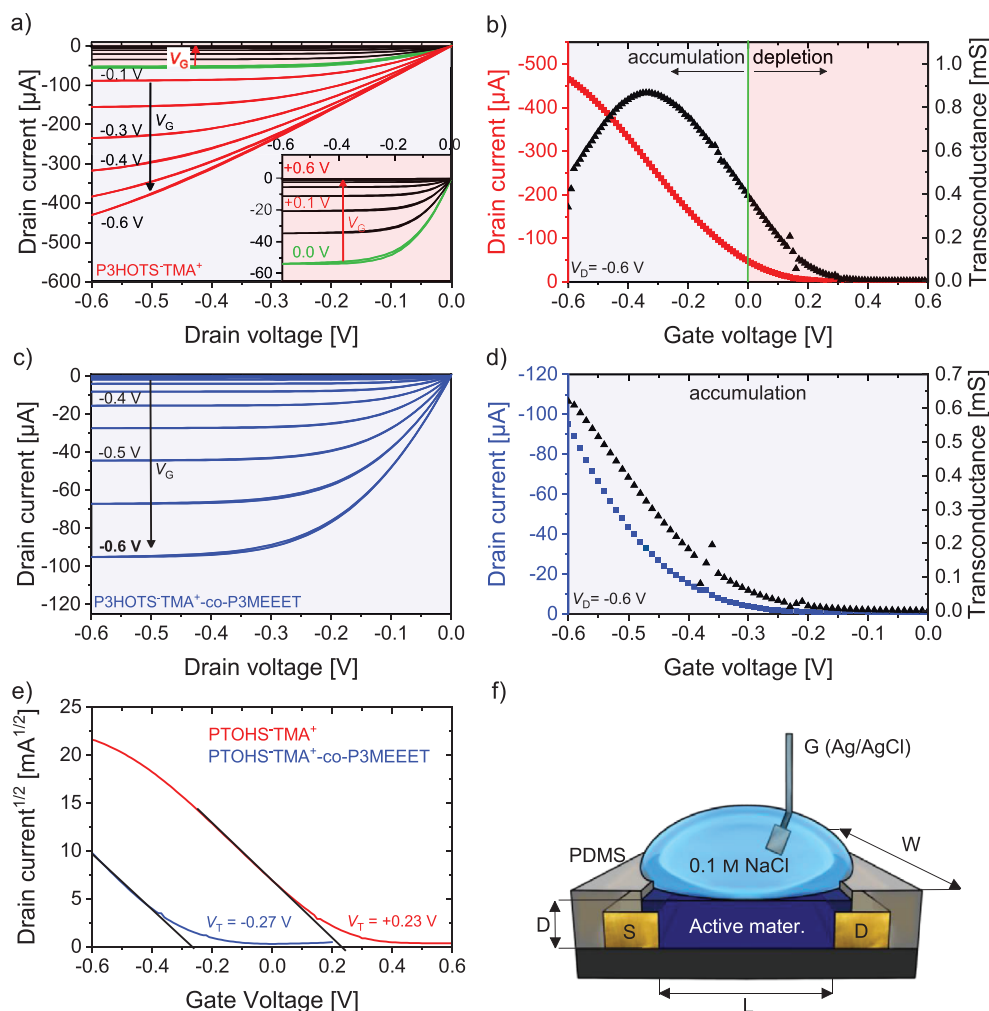


**Figure 4.** OECT characteristics of a device with the geometric parameters  $W = 1.0 \text{ mm } \mu\text{m}$ ,  $L = 5 \text{ } \mu\text{m}$ , and  $D = 69.1 \text{ nm}$  (for P3HOTS-TMA<sup>+</sup>) or  $D = 134 \text{ nm}$  (for P3HOTS-TMA<sup>+</sup>-co-P3MEEET). a) Output characteristics for P3HOTS-TMA<sup>+</sup> at  $V_G$  from 0 to +0.6 V and from 0 to -0.6 V in 100 mV steps. The inset shows the magnification of the depletion mode regime; b) transfer characteristics of P3HOTS-TMA<sup>+</sup>; c) output characteristics for P3HOTS-TMA<sup>+</sup>-co-P3MEEET varying  $V_G$  from 0 to -0.6 V in 100 mV steps; d) transfer characteristics of P3HOTS-TMA<sup>+</sup>-co-P3MEEET; e) square root of the drain current against gate voltage to determine  $V_T$ ; f) schematic illustration of an OECT with source (S), drain (D), gate (G), and the geometric parameters ( $W$ ,  $D$ , and  $L$ ).

prepared film of P3HOTS-TMA<sup>+</sup> is retained even after 70 days in the air. We did not observe any physical changes of the thin films during the storage for 70 days in air as shown by optical micrographs in Figure S17b, Supporting Information). The high conductivity values of P3HOTS-TMA<sup>+</sup>-co-P3MEEET remained almost constant within experimental errors. The long term stability of our system is similar to those copolymer polyelectrolytes containing alkoxy thiophene and EDOT carrying sulfonate groups.<sup>[33]</sup>

As indicated by the SEC measurements, the polymers exhibit a reversible electrochemical redox behavior in an aqueous electrolyte, enabling their investigation as active material in OECTs. For this, the polymers were coated onto prefabricated OECT substrates containing different channel lengths of 5 and 15  $\mu\text{m}$  as described in the methods section in the Supporting Information. The output and transfer characteristics for 15  $\mu\text{m}$  channel length in Figure 4a,b for P3HOTS-TMA<sup>+</sup> show a clear depletion mode behavior (see inset in Figure 4a for the range of gate bias

from 0 to +0.6 V), evident by the high drain current at zero gate voltage, which is  $I_D = 47 \text{ } \mu\text{A}$ , extracted from the transfer characteristics (Figure 4b). The application of positive gate voltages results in a decrease in drain current due to dedoping until the transistor reaches the OFF state at  $V_G = +0.6 \text{ V}$  (Figure 4a, inset).<sup>[56]</sup> On the other hand, applying negative gate voltages to the self-doped sample leads to a drastic increase in drain current up to  $I_{D, \text{max}} = 465 \text{ } \mu\text{A}$  (at  $V_G = -0.6 \text{ V}$ ). However, the output curves lose their clear saturation behavior upon application of high negative gate voltages above  $V_G = -0.4 \text{ V}$  and the output curves show ohmic linear nature. The observation of clear linear regime, and a saturation regime are typical for a transistor output characteristic, whereas ohmic behavior is observed in heavily doped systems and states. This behavior is also observed for PEDOT-S when it gets further oxidized in an OECT.<sup>[30]</sup> This implies a dual mode or hybrid mode operation (both depletion and accumulation modes) in the  $V_G$  range of = +0.6 to -0.4 V. According to the transistor Equation (1) with the geometric parameters, width ( $W$ ),

**Table 1.** Overview of the OECT-data for channel length 5  $\mu\text{m}$  and the electronic properties of the polymers.

Polymer	$I_{\text{max}}$ [ $\mu\text{A}$ ]	$g_{\text{m,max.}}$ [ $\text{mS}^{\text{a}}$ ]	$g_{\text{m,max}}$ [ $\text{S cm}^{-1}$ ] <sup>a)</sup>	$\mu C^*$ [ $\text{F cm}^{-1} \text{V}^{-1} \text{s}^{-1}$ ] <sup>b)</sup>	$V_{\text{T}}$ [V]	HIB [eV] <sup>c)</sup>	IP <sub>CV</sub> [eV] <sup>d)</sup> (undoped)
P3HOTS-TMA <sup>+</sup>	464	0.86	125	1.38	+0.23	0.02	-4.87
P3HOTS-TMA <sup>+</sup> -co-P3MEEET	95.2	0.58	43.9	0.856	-0.27	0.21	-5.16 <sup>e)</sup>
P3MEEET (reference)	47.3	0.66	43.7	2.50	-0.43	0.54	-5.27

<sup>a)</sup> extracted from the first derivation drain current against the gate voltage (output characteristics, at  $V_{\text{D}} = -0.6$  V) and is given as the absolute value and normalized to the film thickness for better comparison; <sup>b)</sup> determined from the slope of the linear fit of  $g_{\text{m}}$  against  $WD/L(V_{\text{T}} - V_{\text{G}})$  given in Figures S19 and S20 (Supporting Information); <sup>c)</sup> obtained by measuring the SECO and VBM to estimate the  $W_{\text{F}}$  and IP with UPS (HIB =  $\text{IP}_{\text{UPS}} - W_{\text{F}}$ ); <sup>d)</sup> IP was calculated from the halfway potentials measured for the pristine (undoped) polymers using CV in thin films on Pt-sputtered ITO substrates in acetonitrile; <sup>e)</sup> calculated from the peak potential obtained from DPV measurements (details are given in the Supporting Information).

thickness ( $D$ ), and length ( $L$ ), charge carrier mobility ( $\mu$ ) and volumetric capacitance ( $C^*$ )

$$g_{\text{m}} = \frac{\partial I_{\text{D}}}{\partial V_{\text{G}}} = \frac{WD}{L} \mu C^* (V_{\text{T}} - V_{\text{G}}) \quad (1)$$

the transconductance  $g_{\text{m}}$ , is defined as the first derivative of the drain current  $I_{\text{D}}$  with respect to  $V_{\text{G}}$  and the maximum value is determined to be  $g_{\text{m}} = 0.87$  mS at  $V_{\text{G}} = -0.33$  V in the accumulation mode range of operation.

Very interestingly, the copolymer displays a full accumulation mode behavior in the OECT device operation range of 0 to  $-0.6$  V gate bias (Figure 4c,d), despite the high degree of the observed self-doping of the copolymer. The output curves show well-defined accumulation curves with a clearly pronounced saturation at higher drain voltages. The maximum transconductance for the device with P3HOTS-TMA<sup>+</sup>-co-P3MEEET is  $g_{\text{m}} = 0.58$  mS at  $V_{\text{G}} = -0.6$  V, where the maximum drain current is  $I_{\text{D,max.}} = 95$   $\mu\text{A}$ . Thus, the drain current is decreased here by a factor of 5 with only a negligible decrease in transconductance compared to the heavily doped homopolymer, P3HOTS-TMA<sup>+</sup>. The threshold voltage  $V_{\text{T}}$  was determined from the plot of the square root of  $I_{\text{D}}$  against the gate voltage by drawing tangents of the linear fit at  $\text{sqrt}(I_{\text{D}}) = 0$  (Figure 4e). For the homopolymer P3HOTS-TMA<sup>+</sup>, we obtain a positive threshold of  $V_{\text{T}} = +0.23$  V. Whereas for the copolymer P3HOTS-TMA<sup>+</sup>-co-P3MEEET it is determined as  $V_{\text{T}} = -0.27$  V, which in total means a shift of 0.50 V compared to the P3HOTS-TMA<sup>+</sup>. On comparing the threshold voltage of the copolymer with the P3MEEET homopolymer ( $V_{\text{T}} = -0.43$  V, Figure S19, Supporting Information) both in accumulation mode operation, this indicates a significant shift of almost 0.2 V toward zero gate bias in the copolymer. Therefore, our study clearly shows that copolymerization using self-dopable monomer promises to be an elegant and suitable tool for shifting the threshold voltage of well-known conjugated homopolymers such as P3MEEET toward zero gate bias. Table 1 summarizes the measured values for  $L = 5$   $\mu\text{m}$ . Further OECT values obtained from the  $L = 5$   $\mu\text{m}$  channels such as the  $I_{\text{D}}$  (ON/OFF) ratio, thickness etc. can be found in the Supporting Information (Table S2 and Figure S20, Supporting Information). The OECT data for the 15  $\mu\text{m}$  channel length is given in Figure S21 (Supporting Information). The threshold voltage values for both 5 and 15  $\mu\text{m}$  channel remain the same for all the samples.

We investigated the OECT response time  $\tau_{\text{ON}}$  of P3HOTS-TMA<sup>+</sup> and P3HOTS-TMA<sup>+</sup>-co-P3MEEET devices (Figure S22, Supporting Information). The response time  $\tau_{\text{ON}}$  of P3HOTS-TMA<sup>+</sup> upon electrochemical oxidation in accumulation mode was with  $\tau_{\text{ON}} = 257$   $\mu\text{s}$  faster than for reduction in depletion mode ( $\tau_{\text{ON}} = 583$   $\mu\text{s}$ ). The copolymer P3HOTS-TMA<sup>+</sup>-co-P3MEEET shows response time  $\tau_{\text{ON}}$  of 571  $\mu\text{s}$ , which is comparable to the homopolymer in depletion mode. Both polymers show response time values in the 10 kHz region close to those of optimized PEDOT:PSS devices for neuromorphic computing or electrophysiological sensing.<sup>[57,58]</sup> This fast response time may be an effect of the attached sulfonate anions, which are immediately available to stabilize the positive charges of the backbone.

To understand the OECT onset voltages as well as inversion from depletion to accumulation mode in copolymer (despite the high degree of self-doping of the copolymer), we examined the charge carrier density ( $n$ ) in thin films of both CPEs by solid-state Mott-Schottky analysis of metal-insulator polymer devices (see Supporting Information for the description of the method and measurement details in Section S3.13, Supporting Information). This resulted in  $n = 1.42 \pm 0.22 \times 10^{21}$   $\text{cm}^{-3}$  for the homopolymer and  $n = 2.7 \pm 0.52 \times 10^{20}$   $\text{cm}^{-3}$  for the copolymer (Figure S23, Supporting Information). The decrease by one order of magnitude in the charge carrier concentration from  $10^{21}$  to  $10^{20}$   $\text{cm}^{-3}$  is caused by decreasing the content of self-dopable moiety P3HOTS-TMA<sup>+</sup> in the copolymer and this appears to be sufficient to change the mode of operation from depletion to accumulation mode. In addition, ultraviolet photoelectron spectroscopy (UPS) was used to determine the second electron cut-off (SECO), the valence band maximum (VBM), and thus work function ( $W_{\text{F}}$ ) for the different polymers (Figure 5a; and Table S2, Supporting Information). It is to be noted that the UPS values correspond to self-doped samples (in partially oxidized form) for P3HOTS-TMA<sup>+</sup> and P3HOTS-TMA<sup>+</sup>-co-P3MEEET, whereas pristine (undoped) form was used for P3MEEET. As expected, the doped polymers exhibit higher ionization potential values compared to the pristine P3MEEET. Very interestingly, the measurements also reveal a steady decrease in the hole injection barrier (HIB) starting from undoped P3MEEET homopolymer with HIB = 0.54 to 0.21 eV for self-doped P3HOTS-TMA<sup>+</sup>-co-P3MEEET and finally to HIB = 0.02 eV for heavily self-doped P3HOTS-TMA<sup>+</sup>. These values clearly support the p-doped nature of the latter two polymers. Additionally, one can assume that the



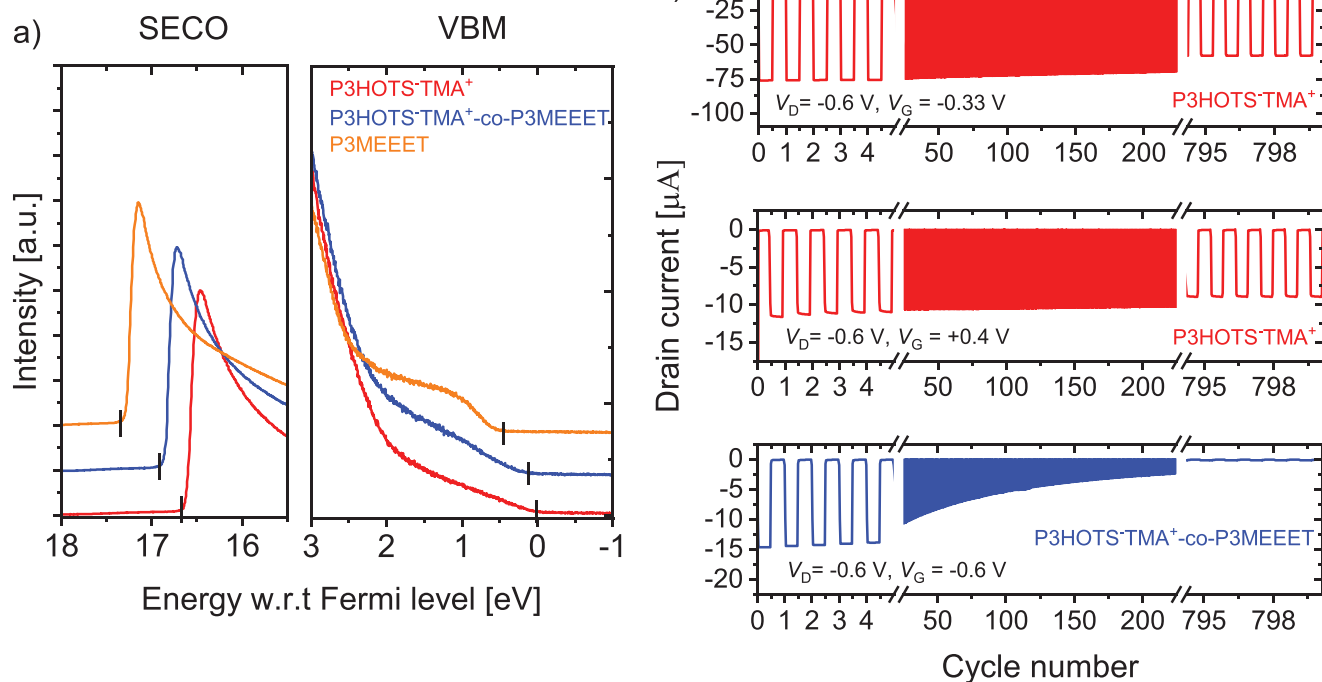


**Figure 5.** a) UPS spectra of the self-doped polymers and P3MEEET with secondary electron cutoff (left) and valence band maximum (right); b) OECT cycling experiments of P3HOTS-TMA<sup>+</sup> in both accumulation and depletion mode operation and P3HOTS-TMA<sup>+</sup>-co-P3MEEET on channels with the geometry  $W = 1.0$  mm,  $L = 15$  μm, and 0.1 M NaCl<sub>aq</sub> as the electrolyte. The drain voltage for all experiments was kept constant at  $V_D = -0.6$  V. Simultaneously, an alternating gate voltage was applied for 2 seconds at  $V_G = 0.0$  V followed by 2 seconds at  $V_G = -0.33$  V,  $V_G = +0.4$  V, or  $V_G = -0.6$  V.

presence of 40 mol% of self-dopable monomer in the copolymer P3HOTS-TMA<sup>+</sup>-co-P3MEEET fills the deep traps and allows the copolymer to function as a better charge transport material with low  $V_T$ , small HIB and high charge carrier concentration compared to the non-doped P3MEEET.

In addition to the transfer and output OECT characteristics, we performed long-time cycle stability measurements of OECTs. Notably, the maximum transconductance of P3HOTS-TMA<sup>+</sup> is observed at  $V_G = -0.33$  V. Therefore, cycling of the self-doped homopolymer in the accumulation regime was conducted by switching between  $V_G = 0.0$  and  $-0.33$  V. Conversely, for depletion mode the same was performed between  $V_G = 0.0$  and  $+0.4$  V, slightly above the threshold voltage. Both modes of operation demonstrate high cycling stabilities with a loss of 20% in drain current observed after 620 cycles in accumulation mode and approximately after 630 cycles in depletion mode, as detailed in Table S3 (Supporting Information). Figure S24 (Supporting Information) also shows the cycling experiments of the CPE homopolymer at  $+0.6$  and  $-0.6$  V gate voltage. On the other hand, the copolymer shows much lower stability with a loss of 20% in drain current after already 18 cycles, comparable to the reference material P3MEEET (14 cycles, Figure S24, Supporting Information). The negative influence of ethylene glycol side chains on cycling stability has already been described in the literature.<sup>[59–62]</sup> The cycling stability can be improved by selecting stable comonomers other than 3MEEET, since copolymerization can be extended to many efficient and stable homopolymers.

### 3. Conclusion

To conclude, we demonstrated a controlled synthesis of a homopolymer and a copolymer as self-doped and solution-processable conjugated polyelectrolytes.

In the self-doped CPEs, self-compensation of charges on the main chain is achieved by the counter ions on side chains without the need of any external molecular dopants. We showed that the degree of doping and thus the electrochemical properties can be tuned by copolymerization with a not self-dopable comonomer. Thin films of both self-doped CPEs exhibit high conductivity values and stability of the doped state in aqueous electrolytes. Beyond that, electrical conductivity measurements show long-term stability when stored under atmospheric conditions. The concept of copolymerization enabled us to switch the mode of operation in p-type OECTs from depletion mode with a threshold voltage of  $V_T = +0.27$  V to accumulation mode with an exceptionally low threshold voltage of  $V_T = -0.23$  V and fast response times. This shift of mode of operation could be attributed to the copolymer strategy which leads to a reduction in the free charge carrier density by one order of magnitude. Additionally, if the self-doped copolymer polyelectrolyte is compared to the reference polymer P3MEEET, the copolymerization leads to small HIB and a considerable threshold voltage shift toward low values. Thus, our study precisely demonstrates that employing self-dopable monomers in copolymerization serves as an effective strategy for changing mode of operation as well as modulating the threshold voltage of

OMIECs toward zero gate bias, a critical requirement for future applications in neuromorphic computing and biosensing.

#### 4. Experimental Section

All details regarding monomer/polymer synthesis and characterization methods are provided in the Supporting Information.

#### Supporting Information

Supporting Information is available from the Wiley Online Library or from the author.

#### Acknowledgements

Funding from Deutsche Forschungsgemeinschaft (DFG, German Research Foundation) under the project numbers 459614649 (Th 807/12-1) and GRK 2817/1 (OPTExC) is kindly acknowledged. The XPS/UPS facility (PHI 5000 VersaProbe III system) at the KeyLab Device Engineering in Bavarian Polymer Institute, Bavarian state ministry for science and art (Soltech) as well as the support of Clara Marx for illustration of the OECT sketch are also acknowledged.

#### Conflict of Interest

The authors declare no conflict of interest.

#### Data Availability Statement

The data that support the findings of this study are available from the corresponding author upon reasonable request.

#### Keywords

bioelectronics, conjugated polyelectrolytes, copolymer, polythiophene, self-compensation

Received: April 25, 2024  
Revised: July 10, 2024  
Published online: July 24, 2024

- [1] S. Inal, G. G. Malliaras, J. Rivnay, *Nat. Commun.* **2017**, *8*, 1767.  
[2] B. D. Paulsen, K. Tybrandt, E. Stavrinidou, J. Rivnay, *Nat. Mater.* **2020**, *19*, 13.  
[3] A. Marks, S. Griggs, N. Gasparini, M. Moser, *Adv. Mater.* **2022**, *9*, 2102039.  
[4] W. Huang, J. Chen, Y. Yao, D. Zheng, X. Ji, L.-W. Feng, D. Moore, N. R. Glavin, M. Xie, Y. Chen, R. M. Pankow, A. Surendran, Z. Wang, Y. Xia, L. Bai, J. Rivnay, J. Ping, X. Guo, Y. Cheng, T. J. Marks, A. Facchetti, *Nature* **2023**, *613*, 496.  
[5] R. B. Rashid, X. Ji, J. Rivnay, *Biosens. Bioelectron.* **2021**, *190*, 113461.  
[6] H.-Y. Wu, J.-D. Huang, S. Y. Jeong, T. Liu, Z. Wu, T. van der Pol, Q. Wang, M.-A. Stoeckel, Q. Li, M. Fahlman, D. Tu, H. Y. Woo, C.-Y. Yang, S. Fabiano, *Mater. Horiz.* **2023**, *10*, 4213.  
[7] P. C. Harikeesh, C.-Y. Yang, D. Tu, J. Y. Gerasimov, A. M. Dar, A. Armada-Moreira, M. Massetti, R. Kroon, D. Bliman, R. Olsson, E. Stavrinidou, M. Berggren, S. Fabiano, *Nat. Commun.* **2022**, *13*, 901.

- [8] R. Bhunia, E. K. Boahen, D. J. Kim, H. Oh, Z. Kong, D. H. Kim, *J. Mater. Chem. C* **2023**, *11*, 7485.  
[9] D. A. Bernards, G. G. Malliaras, *Adv. Funct. Mater.* **2007**, *17*, 3538.  
[10] J. Rivnay, P. Leleux, M. Sessolo, D. Khodagholy, T. Hervé, M. Flocchi, G. G. Malliaras, *Adv. Mater.* **2013**, *25*, 7010.  
[11] S. Inal, J. Rivnay, P. Leleux, M. Ferro, M. Ramuz, J. C. Brendel, M. M. Schmidt, M. Thelakkat, G. G. Malliaras, *Adv. Mater.* **2014**, *26*, 7450.  
[12] Y. Yao, W. Huang, J. Chen, X. Liu, L. Bai, W. Chen, Y. Cheng, J. Ping, T. J. Marks, A. Facchetti, *Adv. Mater.* **2023**, *35*, 2209906.  
[13] A. M. Pappa, D. Ohayon, A. Giovannitti, I. P. Maria, A. Savva, I. Uguz, J. Rivnay, I. McCulloch, R. M. Owens, S. Inal, *ScienceSci. Adv.* **2018**, *4*, aat0911.  
[14] Y. Xuan, M. Sandberg, M. Berggren, X. Crispin, *Org. Electron.* **2012**, *13*, 632.  
[15] S. T. Keene, A. Melianas, Y. van de Burgt, A. Salleo, *Adv. Electron. Mater.* **2019**, *5*, 1800686.  
[16] M. M. Schmidt, M. ElMahmoudy, G. G. Malliaras, S. Inal, M. Thelakkat, *Macromol. Chem. Phys.* **2018**, *219*, 1700374.  
[17] C. B. Nielsen, A. Giovannitti, D.-T. Sbircea, E. Bandiello, M. R. Niazi, D. A. Hanifi, M. Sessolo, A. Amassian, G. G. Malliaras, J. Rivnay, I. McCulloch, *J. Am. Chem. Soc.* **2016**, *138*, 10252.  
[18] S. T. Keene, T. P. A. van der Pol, D. Zakhidov, C. H. L. Weijtens, R. A. J. Janssen, A. Salleo, Y. van de Burgt, *Adv. Mater.* **2020**, *32*, 2000270.  
[19] S. E. Doris, A. Pierre, R. A. Street, *Adv. Mater.* **2018**, *30*, 1706757.  
[20] H. Tseng, A. Weissbach, J. Kucinski, A. Solgi, R. Nair, L. M. Bongartz, G. Ciccone, M. Cucchi, K. Leo, H. Kleemann, *Adv. Mater. Interfaces* **2023**, *10*, 2201914.  
[21] S. T. M. Tan, G. Lee, I. Denti, G. LeCroy, K. Rozylowicz, A. Marks, S. Griggs, I. McCulloch, A. Giovannitti, A. Salleo, *Adv. Mater.* **2022**, *34*, 2202359.  
[22] A. Giovannitti, R. B. Rashid, Q. Thiburce, B. D. Paulsen, C. Cendra, K. Thorley, D. Moia, J. T. Mefford, D. Hanifi, D. Weiyan, M. Moser, A. Salleo, J. Nelson, I. McCulloch, J. Rivnay, *Adv. Mater.* **2020**, *32*, 1908047.  
[23] A. Giovannitti, D.-T. Sbircea, S. Inal, C. B. Nielsen, E. Bandiello, D. A. Hanifi, M. Sessolo, G. G. Malliaras, I. McCulloch, J. Rivnay, *Proc. Natl. Acad. Sci. USA* **2016**, *113*, 12017.  
[24] J. C. Brendel, M. M. Schmidt, G. Hagen, R. Moos, M. Thelakkat, *Chem. Mater.* **2014**, *26*, 1992.  
[25] A. O. Patil, Y. Ikenoue, N. Basescu, N. Colaneri, J. Chen, F. Wudl, A. J. Heeger, *Synth. Met.* **1987**, *20*, 151.  
[26] M. Chayer, K. Faid, M. Leclerc, *Chem. Mater.* **1997**, *9*, 2902.  
[27] G. Zotti, S. Zecchin, G. Schiavon, L. Groenendaal, *Macromol. Chem. Phys.* **2002**, *203*, 1958.  
[28] R. H. Karlsson, A. Herland, M. Hamedi, J. A. Wigenius, A. Åslund, X. Liu, M. Fahlman, O. Inganäs, P. Konradsson, *Chem. Mater.* **2009**, *21*, 1815.  
[29] H. Yano, K. Kudo, K. Marumo, H. Okuzaki, *Sci. Adv.* **2019**, *5*, aav9492.  
[30] E. Zeglio, J. Eriksson, R. Gabrielsson, N. Solin, O. Inganäs, *Adv. Mater.* **2017**, *29*, 1605787.  
[31] E. Zeglio, M. Vagin, C. Musumeci, F. N. Ajjan, R. Gabrielsson, X. T. Trinh, N. T. Son, A. Maziz, N. Solin, O. Inganäs, *Chem. Mater.* **2015**, *27*, 6385.  
[32] E. Zeglio, M. M. Schmidt, M. Thelakkat, R. Gabrielsson, N. Solin, O. Inganäs, *Chem. Mater.* **2017**, *29*, 4293.  
[33] C. Beaumont, J. Turgeon, M. Idir, D. Neusser, R. Lapointe, S. Caron, W. Dupont, D. D'Astous, S. Shamsuddin, S. Hamza, É. Landry, S. Ludwigs, M. Leclerc, *Macromolecules* **2021**, *54*, 5464.  
[34] C.-K. Mai, H. Zhou, Y. Zhang, Z. B. Henson, T.-Q. Nguyen, A. J. Heeger, G. C. Bazan, *Angew. Chem., Int. Ed.* **2013**, *52*, 12874.  
[35] T. Nguyen-Dang, S. Chae, J. Chatsirisupachai, H. Wakidi, V. Promarak, Y. Visell, T.-Q. Nguyen, *Adv. Mater.* **2022**, *34*, 2200274.

- [36] L. C. Llanes, A. T. Lill, Y. Wan, S. Chae, A. Yi, T. Nguyen-Dang, H. J. Kim, L. Sepunaru, J. Read de Alaniz, G. Lu, G. C. Bazan, T.-Q. Nguyen, *J. Mater. Chem. C* **2023**, *11*, 8274.
- [37] P. Schmode, A. Savva, R. Kahl, D. Ohayon, F. Meichsner, O. Dolynchuk, T. Thurn-Albrecht, S. Inal, M. Thelakkat, *ACS Appl. Mater. Interfaces* **2020**, *12*, 13029.
- [38] E. E. Sheina, J. Liu, M. C. Iovu, D. W. Laird, R. D. McCullough, *Macromolecules* **2004**, *37*, 3526.
- [39] R. H. Lohwasser, M. Thelakkat, *Macromolecules* **2011**, *44*, 3388.
- [40] Y.-L. Yang, Y.-H. Lee, Y.-P. Lee, C.-J. Chiang, C. Shen, C.-C. Wu, Y. Ohta, T. Yokozawa, C.-A. Dai, *Polym. Int.* **2014**, *63*, 2068.
- [41] E. E. Sheina, S. M. Khersonsky, E. G. Jones, R. D. McCullough, *Chem. Mater.* **2005**, *17*, 3317.
- [42] P. Schmode, K. Schötz, O. Dolynchuk, F. Panzer, A. Köhler, T. Thurn-Albrecht, M. Thelakkat, *Macromolecules* **2020**, *53*, 2474.
- [43] J. L. Bredas, G. B. Street, *Acc. Chem. Res.* **1985**, *18*, 309.
- [44] C. Enengl, S. Enengl, S. Pluczyk, M. Havlicek, M. Lapkowski, H. Neugebauer, E. Ehrenfreund, *ChemPhysChem* **2016**, *17*, 3836.
- [45] P. Schmode, D. Ohayon, P. M. Reichstein, A. Savva, S. Inal, M. Thelakkat, *Chem. Mater.* **2019**, *31*, 5286.
- [46] P. J. Brown, D. S. Thomas, A. Köhler, J. S. Wilson, J.-S. Kim, C. M. Ramsdale, H. Sirringhaus, R. H. Friend, *Phys. Rev. B* **2003**, *67*, 064203.
- [47] J. Clark, C. Silva, R. H. Friend, F. C. Spano, *Phys. Rev. Lett.* **2007**, *98*, 206406.
- [48] C. Scharsich, R. H. Lohwasser, M. Sommer, U. Asawapirom, U. Scherf, M. Thelakkat, D. Neher, A. Köhler, *J. Polym. Sci., Part B: Polym. Phys.* **2012**, *50*, 442.
- [49] K. Fidanovski, M. Gu, L. Travaglini, A. Lauto, D. Mawad, *Adv. Healthcare Mater.* **2023**, *8*, 2302354.
- [50] K. Gräf, M. A. Rahim, S. Das, M. Thelakkat, *Dyes Pigm.* **2013**, *99*, 1101.
- [51] Y. Aoyama, T. Yamanari, T. N. Murakami, T. Nagamori, K. Marumoto, H. Tachikawa, J. Mizukado, H. Suda, Y. Yoshida, *Polym. J.* **2015**, *47*, 26.
- [52] Y. Ikenoue, N. Outani, A. O. Patil, F. Wudl, A. J. Heeger, *Synth. Met.* **1989**, *30*, 305.
- [53] R. J. Mammone, A. G. MacDiarmid, *J. Chem. Soc., Faraday Trans. 1* **1985**, *81*, 105.
- [54] R. K. Singh, J. Kumar, R. Singh, R. Kant, S. Chand, V. Kumar, *Mater. Chem. Phys.* **2007**, *104*, 390.
- [55] N. A. Shahrim, Z. Ahmad, A. Wong Azman, Y. F. Buys, N. Sarifuddin, *Mater. Adv.* **2021**, *2*, 7118.
- [56] J. Rivnay, S. Inal, A. Salleo, R. M. Owens, M. Berggren, G. G. Malliaras, *Nat. Rev. Mater.* **2018**, *3*, 17086.
- [57] S.-K. Lee, Y. W. Cho, J.-S. Lee, Y.-R. Jung, S.-H. Oh, J.-Y. Sun, S. Kim, Y.-C. Joo, *Adv. Sci.* **2021**, *8*, 2001544.
- [58] J. E. Tyrrell, M. G. Boutelle, A. J. Campbell, *Adv. Funct. Mater.* **2021**, *31*, 2007086.
- [59] A. A. Szumska, I. P. Maria, L. Q. Flagg, A. Savva, J. Surgailis, B. D. Paulsen, D. Moia, X. Chen, S. Griggs, J. T. Mefford, R. B. Rashid, A. Marks, S. Inal, D. S. Ginger, A. Giovannitti, J. Nelson, *J. Am. Chem. Soc.* **2021**, *143*, 14795.
- [60] M. Moser, T. C. Hidalgo, J. Surgailis, J. Gladisch, S. Ghosh, R. Sheelamanthula, Q. Thiburce, A. Giovannitti, A. Salleo, N. Gasparini, A. Wadsworth, I. Zozoulenko, M. Berggren, E. Stavrinidou, S. Inal, I. McCulloch, *Adv. Mater.* **2020**, *32*, 2002748.
- [61] Y. Wang, E. Zeglio, H. Liao, J. Xu, F. Liu, Z. Li, I. P. Maria, D. Mawad, A. Herland, I. McCulloch, W. Yue, *Chem. Mater.* **2019**, *31*, 9797.
- [62] M. Xie, H. Liu, M. Wu, C. Chen, J. Wen, L. Bai, J. Yu, W. Huang, *Org. Electron.* **2023**, *117*, 106777.